On penalty flux parameters in first order DG formulations

Jesse Chan, T. Warburton

Abstract

Abstract goes here. Mention assumptions: continuously varying material data, skew-symmetric formulations.

1 Introduction

Intro

2 Semi-discrete discontinuous Galerkin formulation

We consider linear first order hyperbolic systems of PDEs in $\mathbb{R}^d$

$$\boldsymbol{A}_0(\boldsymbol{x})\frac{\partial \boldsymbol{U}}{\partial t} + \sum_{i=1}^{d} \frac{\partial \left(\boldsymbol{A}_i \boldsymbol{U}\right)}{\partial \boldsymbol{x}_i} = 0 \tag{1}$$

with solution components $\boldsymbol{U} = (u_1, \ldots, u_M)^T$. In this work, we assume that $\boldsymbol{A}_0$ is symmetric and positive-definite, and that the matrices $\boldsymbol{A}_i$ are symmetric or symmetrizable. In this work, we assume that $\boldsymbol{A}_i$ are constant, though $\boldsymbol{A}_0(\boldsymbol{x})$ may vary spatially. These assumptions are true for many PDEs governing wave propagation in heterogeneous media, including such as the acoustic wave equation [1], linear elasticity [2, 3, 4], and Maxwell's equations [5, 6, 7].

We assume the domain Ω is triangulated exactly using a mesh Ω_h consisting of elements D^k. We define the L^2 inner product over elements D^k and their boundaries ∂D^k as

$$(u,v)_{D^k} = \int_{D^k} u(\boldsymbol{x})v(\boldsymbol{x})\,\mathrm{d}x, \qquad \langle u,v\rangle_{\partial D^k} = \int_{\partial D^k} u(\boldsymbol{x})v(\boldsymbol{x})\,\mathrm{d}x.$$

A semi-discrete DG formulation for (1) may be written as

$$\sum_{D^k\in\Omega_h} \left(\boldsymbol{A}_0\frac{\partial \boldsymbol{U}}{\partial t}, \boldsymbol{V}\right)_{L^2(D^k)} = \sum_{D^k\in\Omega_h} \left((\boldsymbol{A}_i(\boldsymbol{U}), \boldsymbol{V}_{,i})_{L^2(D^k)} - \langle (\boldsymbol{A}_n\boldsymbol{U})^*, \boldsymbol{V}\rangle_{\partial D^k}\right) \tag{2}$$

where $(\boldsymbol{A}_n\boldsymbol{U})^*$ is a numerical flux defined on boundary faces and shared faces between elements.

2.1 Penalization terms in numerical fluxes

Let f be a shared face between two elements $D^{k,+}$ and $D^{k,-}$ with outward normal $\boldsymbol{n}^-$ on $D^{k,-}$, and let $\boldsymbol{U}^+, \boldsymbol{U}^-$ be evaluations of $\boldsymbol{U}$ restricted to $D^{k,+}$ and $D^{k,-}$, respectively. The average of both scalar and vector-valued functions is defined as

$$\{\{u\}\} = \frac{u^+ + u^-}{2},$$

and the jump of scalar and vector-valued functions over f are defined as

$$[\![u]\!] = u^+\boldsymbol{n}^+ + u^-\boldsymbol{n}^-, \qquad [\![\boldsymbol{u}]\!] = \boldsymbol{u}^+\cdot\boldsymbol{n}^+ + \boldsymbol{u}^-\cdot\boldsymbol{n}^-.$$

Typical numerical fluxes are defined as the sum of the average of $\boldsymbol{U}^+$ and $\boldsymbol{U}^-$ and a penalization term $\boldsymbol{G}(\boldsymbol{U}^+, \boldsymbol{U}^-)$

$$(\boldsymbol{A}_n \boldsymbol{U})^* = \{\{\boldsymbol{A}_n \boldsymbol{U}\}\} \cdot \boldsymbol{n}^- - \boldsymbol{G}(\boldsymbol{U}^+, \boldsymbol{U}^-). \tag{3}$$

Clean up jump notation here. The upwind numerical flux is a well-known flux of the form (3). For an outward normal vector $\boldsymbol{n}^-$, let $\boldsymbol{A}_n = \sum_{i=1}^d \boldsymbol{A}_i \boldsymbol{n}_i^-$. By symmetry of $\boldsymbol{A}_i$, $\boldsymbol{A}_n$ contains real eigenvalues, and admits an eigenvalue decomposition

$$\boldsymbol{A}_n = \boldsymbol{V} \boldsymbol{\Lambda} \boldsymbol{V}^T, \qquad \boldsymbol{\Lambda} = \begin{pmatrix} \lambda_1 & & \\ & \ddots & \\ & & \lambda_d \end{pmatrix}.$$

For problems with continuous coefficients, the upwind numerical flux over a face $f \in \Gamma_h$ can be defined as

$$(\boldsymbol{A}_n \boldsymbol{U})^* = \boldsymbol{A}_n^+ \boldsymbol{U}^- + \boldsymbol{A}_{\boldsymbol{n}}^- \boldsymbol{U}^+,$$

where the matrices $\boldsymbol{A}_{\boldsymbol{n}}^+, \boldsymbol{A}_{\boldsymbol{n}}^-$ are constructed from the positive and negative eigenvalues

$$\boldsymbol{A}_n^+ = \frac{1}{2} \boldsymbol{V} \left(\boldsymbol{\Lambda} + |\boldsymbol{\Lambda}| \right) \boldsymbol{V}^T$$
$$\boldsymbol{A}_n^- = \frac{1}{2} \boldsymbol{V} \left(\boldsymbol{\Lambda} - |\boldsymbol{\Lambda}| \right) \boldsymbol{V}^T,$$

and $|\boldsymbol{\Lambda}|$ is the diagonal matrix whose entries consist of the absolute values of the eigenvalues $|\lambda_i|$. This can be rewritten as the sum of the central flux and a penalization

$$(\boldsymbol{A}_n \boldsymbol{U})^* = \{\{\boldsymbol{A}_n \boldsymbol{U}\}\} - \boldsymbol{V} |\boldsymbol{\Lambda}| \boldsymbol{V}^T [\![\boldsymbol{U}]\!].$$

We consider penalty fluxes as an alternative to upwind fluxes, which penalize appropriately defined jumps of the solution. One such penalty flux is

$$(\boldsymbol{A}_n \boldsymbol{U})^* = \{\{\boldsymbol{A}_n \boldsymbol{U}\}\} - \frac{\tau}{2} \boldsymbol{A}_n^T [\![\boldsymbol{A}_n \boldsymbol{U}]\!].$$

where τ is proportional to $\lambda_{\max}^{-1}$. This choice of τ ensures that the penalty term is of the same order of magnitude as the upwind penalization, and that the CFL restriction for both upwind and penalty fluxes are identical. Unlike upwind fluxes, penalty fluxes can be used when a diagonalization of $\boldsymbol{A}_n$ is not explicitly known, such as linear elasticity in anisotropic media [4].

3 Dependence of spectra on the penalty parameter

The remainder of this work focuses on the influence of τ on the spectra of DG discretization matrices.

3.1 Conforming and non-conforming spaces

Let V denote the piecewise polynomial approximation space

$$V = \left\{ \boldsymbol{U} \in \left(L^2(\Omega) \right)^d : \boldsymbol{U}|_{D^k} \in \left(P^N(D^k) \right)^d \right\}.$$

We define a decomposition of V into a conforming part V^C and a non-conforming part V^{NC} based on the penalization term $\boldsymbol{G}(\boldsymbol{U}^+, \boldsymbol{U}^-)$. The conforming part is defined as the null space of $\boldsymbol{G}(\boldsymbol{U}^+, \boldsymbol{U}^-)$

$$V^C = \left\{ \boldsymbol{U}(\boldsymbol{x}) \in V : \quad \boldsymbol{G}(\boldsymbol{U}^+, \boldsymbol{U}^-) = 0, \quad \forall f \in \Gamma_h \right\}, \tag{4}$$

while the non-conforming approximation space V^{NC} is defined as L^2 orthogonal complement of V^C in V

$$V^{NC} = \left\{ \boldsymbol{U}(\boldsymbol{x}) \in V : (\boldsymbol{u}, \boldsymbol{v})_{L^2(\Omega)} = 0, \quad \forall \boldsymbol{v} \in V^C \right\}.$$

When the coefficient matrices $\boldsymbol{A}_i$ are spatially continuous, the upwind flux condition $\boldsymbol{V} |\boldsymbol{\Lambda}| \boldsymbol{V}^T [\![\boldsymbol{U}]\!] = 0$ and the penalty flux condition $\boldsymbol{A}_n^T [\![\boldsymbol{A}_n \boldsymbol{U}]\!] = 0$ are both equivalent to

$$\boldsymbol{v}_i^T [\![\boldsymbol{U}]\!] = 0, \qquad \lambda_i \neq 0,$$

where $\lambda_i, \boldsymbol{v}_i$ are an eigenvalue and eigenvector of $\boldsymbol{A}_n$. As a result, the conforming and non-conforming spaces induced by upwind and penalty fluxes are identical.

For problems with discontinuous material data, it is less straightforward to show equivalence between the conforming spaces V^C resulting from upwind and penalty fluxes. However, for many practical wave propagation settings, spatially varying coefficients are incorporated into the matrix $\boldsymbol{A_0}$, resulting in constant $\boldsymbol{A}_i$. For both smoothly varying and discontinuous $\boldsymbol{A}_0$, it is possible to formulate energy stable DG methods with penalty fluxes [8, 1]. Additionally, DG methods using penalty fluxes are observed to perform similarly to DG methods with upwind fluxes for wave propagation problems with discontinuous coefficients [7, 1, 4].

3.2 Scalar advection and acoustic wave propagation

We illustrate the conforming spaces induced by penalty fluxes using the scalar advection equation and acoustic wave equation as concrete examples. The scalar advection equation is given as

$$\frac{\partial u}{\partial t} + \cdot (\boldsymbol{\beta} u) = 0.$$

where $\boldsymbol{\beta}$ is the direction of advection. For continuous advection vectors such that $\boldsymbol{\beta}(\boldsymbol{x}) \neq 0$, the penalty flux is equivalent to a parametrized upwind flux [9]

$$(\boldsymbol{A}_n \boldsymbol{U})^* = \{\{\boldsymbol{\beta}_n u\}\} - \tau |\boldsymbol{\beta}_n| [\![u]\!].$$

The conforming space V^C induced by this flux is then

$$V^C = \left\{ u \in L^2(\Omega) : \quad u|_{D^k} \in P^N(D^k), \quad |\boldsymbol{\beta}_n| [\![u]\!] = 0 \right\}.$$

In one dimension, this simply implies that u is C^0-continuous across element boundaries. In higher dimensions, this implies that u is continuous along streamlines or directions $\boldsymbol{d}(\boldsymbol{x})$ where $\boldsymbol{\beta} \cdot \boldsymbol{d} \neq 0$.

Next, we consider the acoustic wave equation in pressure-velocity form

$$\begin{aligned} \frac{1}{c^2} \frac{\partial p}{\partial t} &= \nabla \cdot \boldsymbol{u} \\ \frac{\partial \boldsymbol{u}}{\partial t} &= \nabla p, \end{aligned}$$

where $c^2(\boldsymbol{x})$ is the wavespeed. Let $\boldsymbol{U}$ denote the group variable $\boldsymbol{U} = (p, u, v)$, where u and v are the x and y components of velocity. Then, in two dimensions, the isotropic wave equation is given as

$$\frac{\partial \boldsymbol{U}}{\partial t} + \frac{\partial \boldsymbol{A}_x \boldsymbol{U}}{\partial x} + \frac{\partial \boldsymbol{A}_y \boldsymbol{U}}{\partial y} = 0, \qquad \boldsymbol{A}_x = \begin{pmatrix} 0 & 1 & 0 \\ 1 & 0 & 0 \\ 0 & 0 & 0 \end{pmatrix}, \qquad \boldsymbol{A}_y = \begin{pmatrix} 0 & 0 & 1 \\ 0 & 0 & 0 \\ 1 & 0 & 0 \end{pmatrix}.$$

The normal flux matrix $\boldsymbol{A}_n$ is then

$$\boldsymbol{A}_n = \begin{pmatrix} 0 & \boldsymbol{n}_x^- & \boldsymbol{n}_y^- \\ \boldsymbol{n}_x^- & 0 & 0 \\ \boldsymbol{n}_y^- & 0 & 0 \end{pmatrix}$$

implying that the penalty fluxes are

$$\{\{\boldsymbol{A}_n\boldsymbol{U}\}\} - \frac{\tau}{2}\boldsymbol{A}_n^T[\![\boldsymbol{A}_n\boldsymbol{U}]\!] = \begin{pmatrix} \{\{\boldsymbol{u}_n\}\} \\ \{\{p\}\}\,\boldsymbol{n}_x^- \\ \{\{p\}\}\,\boldsymbol{n}_y^- \end{pmatrix} - \frac{\tau}{2}\begin{pmatrix} [\![p]\!] \\ [\![\boldsymbol{u_n}]\!]\boldsymbol{n}_x^- \\ [\![\boldsymbol{u_n}]\!]\boldsymbol{n}_y^- \end{pmatrix}$$

For $\tau = 1$, these fluxes coincide with the upwind fluxes for continuously varying media. In this case, the conforming subspace V^C induced by the penalty flux consists of a scalar (pressure) component V_p^C and a vector (velocity) component $V_{\boldsymbol{u}}^C$. The pressure component p satisfies $[\![p]\!] = 0$ over all faces $f \in \Gamma_h$. For polynomial approximation spaces, this implies that p is continuous across faces, edges, and vertices, and V_p^C is the standard C^0 continuous piecewise polynomial finite element space.

For the velocity component $V_{\boldsymbol{u}}^C$, the penalty fluxes enforce normal continuity, such that $[\![\boldsymbol{u}]\!] \cdot \boldsymbol{n}^- = 0$ over all faces $f \in \Gamma_h$. Since each component of $\boldsymbol{u}$ is approximated from $P^N(D^k)$, this implies that $V_{\boldsymbol{u}}^C$ is the $H(\mathrm{div})$-conforming Brezzi-Douglas-Marini finite element space [10, 11].[1]

Penalty fluxes can also be interpreted as Lax-Friedrichs fluxes applied to scalar and vector variables separately. In contrast, for a component-wise Lax-Friedrichs flux

$$(\boldsymbol{A}_n\boldsymbol{U})^* = \begin{pmatrix} \{\{\boldsymbol{u}_n\}\} \\ \{\{p\}\}\,\boldsymbol{n}_x^- \\ \{\{p\}\}\,\boldsymbol{n}_y^- \end{pmatrix} - \frac{\tau}{2}\begin{pmatrix} [\![p]\!] \\ [\![\boldsymbol{u}_x]\!] \\ [\![\boldsymbol{u}_y]\!] \end{pmatrix},$$

the conforming velocity space $V_{\boldsymbol{u}}^C$ becomes the space of vector piecewise polynomial functions which are C^0 continuous in both x and y components, resulting in over-constrained continuity conditions for $\boldsymbol{u}$.

3.3 Behavior as $\tau \to \infty$

Let $\boldsymbol{K}$ be the matrix resulting from the discretization of the DG formulation (2). We are interested in eigenvalues and eigenvectors of

$$\boldsymbol{K}\boldsymbol{u} = \lambda_i \boldsymbol{M}\boldsymbol{u}$$

where $\boldsymbol{M}$ is the L^2 mass matrix. We adapt the approach of Warburton and Embree in [13] to (5) to show that the spectra of $\boldsymbol{K}$ splits into two sets of eigenvalues as $\tau \to \infty$, the first of which approaches the eigenvalues of $\boldsymbol{A}$, and the second of which diverges with real part approaching $-\infty$ as $\tau \to \infty$.

Let $\{\boldsymbol{\Phi}_i\}_{i=1}^{N^C}$ and $\{\boldsymbol{\Psi}_i\}_{i=1}^{N^{NC}}$ be L^2-orthogonal bases for $\boldsymbol{V}^C$ and $\boldsymbol{V}^{NC}$, respectively. These spaces then induce a block decomposition of the DG discretization matrix $\boldsymbol{K}$

$$\boldsymbol{K} = \begin{pmatrix} \boldsymbol{A} & \boldsymbol{B} \\ \tilde{\boldsymbol{B}}^T & \boldsymbol{C} + \tau\boldsymbol{S} \end{pmatrix}, \tag{5}$$

where the blocks $\boldsymbol{A}, \boldsymbol{B}, \boldsymbol{C}$ are defined as

$$\begin{aligned}
\boldsymbol{A}_{mn} &= \sum_{D^k \in \Omega_h} \left(\boldsymbol{A}_i\boldsymbol{\Phi}_n, \boldsymbol{\Phi}_{m,i}\right)_{D^k}, \qquad 1 \le m, n \le N^C \\
\boldsymbol{B}_{mn} &= \sum_{D^k \in \Omega_h} \left(\boldsymbol{A}_i\boldsymbol{\Psi}_n, \boldsymbol{\Phi}_{m,i}\right)_{D^k} - \left\langle \{\{\boldsymbol{A}_n\boldsymbol{\Psi}_i\}\}, \boldsymbol{\Phi}_i \right\rangle_{\partial D^k} \qquad 1 \le m \le N^C, \quad 1 \le n \le N^{NC} \\
\boldsymbol{C}_{mn} &= -\sum_{D^k \in \Omega_h} \left\langle \{\{\boldsymbol{A}_n\boldsymbol{\Psi}_i\}\}, \boldsymbol{\Psi}_i \right\rangle_{\partial D^k}, \qquad 1 \le m, n \le N^{NC} \\
\boldsymbol{S}_{mn} &= \frac{1}{2}\sum_{D^k \in \Omega_h} \left\langle \boldsymbol{A}_n^T[\![\boldsymbol{A}_n\boldsymbol{\Psi_n}]\!], \boldsymbol{\Psi}_m \right\rangle_{\partial D^k}, \qquad 1 \le m, n \le N^{NC}.
\end{aligned}$$

[1] It is possible to recover $V_{\boldsymbol{u}}^C$ as the Raviart-Thomas finite element space by approximating each component of $\boldsymbol{u}$ from a smaller polynomial space [12].

For exact quadrature, constant $\boldsymbol{A}_i$, and $\tau = 0$, the DG formulation is skew-symmetric [7, 14, 15], implying that $\boldsymbol{A}, \boldsymbol{C}$ are skew-symmetric and that $\tilde{\boldsymbol{B}} = -\boldsymbol{B}$. Additionally, the entries of the penalization matrix $\boldsymbol{S}$ can be rewritten as

$$\boldsymbol{S}_{mn} = \frac{1}{2} \sum_{D^k \in \Omega_h} \langle [\![\boldsymbol{A}_n \boldsymbol{\Psi}_n]\!], \boldsymbol{A}_n \boldsymbol{\Psi}_m \rangle_{\partial D^k} = -\frac{1}{2} \sum_{f \in \Gamma_h} \langle [\![\boldsymbol{A}_n \boldsymbol{\Psi}_n]\!], [\![\boldsymbol{A}_n \boldsymbol{\Psi}_m]\!] \rangle_f ,$$

implying that $\boldsymbol{S}$ is symmetric and negative-definite.

We may now show how the spectra of $\boldsymbol{K}$ behaves as $\tau \to \infty$. Since $\boldsymbol{A}$ is skew-symmetric and $\boldsymbol{S}$ is symmetric, they are diagonalizable under unitary matrices $\boldsymbol{U}$ and $\boldsymbol{Q}$, whose columns contain the eigenvectors of $\boldsymbol{A}$ and $\boldsymbol{S}$, respectively. Following [13], we apply a block diagonal similarity transform to yield

$$\tilde{\boldsymbol{K}} = \begin{pmatrix} \boldsymbol{U}^* & \\ & \boldsymbol{Q}^* \end{pmatrix} \begin{pmatrix} \boldsymbol{A} & \boldsymbol{B} \\ -\boldsymbol{B}^T & \boldsymbol{C} + \tau \boldsymbol{S} \end{pmatrix} \begin{pmatrix} \boldsymbol{U} & \\ & \boldsymbol{Q} \end{pmatrix} = \begin{pmatrix} \boldsymbol{\Lambda}^C & \boldsymbol{U}^* \boldsymbol{B} \boldsymbol{Q} \\ -\boldsymbol{Q}^* \boldsymbol{B}^T \boldsymbol{U} & \boldsymbol{Q}^* \boldsymbol{C} \boldsymbol{Q} + \tau \boldsymbol{\Lambda}^S \end{pmatrix},$$

where $\boldsymbol{\Lambda}^C, \boldsymbol{\Lambda}^S$ are diagonal matrices whose entries consist of eigenvalues of $\boldsymbol{A}$ and $\boldsymbol{S}$.

Since $\boldsymbol{Q}^* \boldsymbol{C} \boldsymbol{Q}$ is skew-symmetric and its diagonal has zero real part, $\boldsymbol{Q}^* \boldsymbol{C} \boldsymbol{Q} + \tau \boldsymbol{\Lambda}^S$ has diagonal entries $\tau \lambda_j^S + \mathrm{i}\gamma_j$, where λ_j^S is real and negative and γ_j is independent of τ. Thus, the diagonal of $\tilde{\boldsymbol{K}}$ consists of N^C purely imaginary values and N^{NC} values of the form $\tau \lambda_j^S + \mathrm{i}\gamma_j$. Since $\boldsymbol{B}$ is independent of τ, the entries of $\boldsymbol{U}^* \boldsymbol{B} \boldsymbol{Q}$ are independent of τ, assuming that $\boldsymbol{U}$ and $\boldsymbol{Q}$ are normalized. Gerschgorin's theorem applied to $\tilde{\boldsymbol{K}}$ then implies that the eigenvalues of $\boldsymbol{K}$ are contained in two sets of discs with radii independent of τ. The first set of discs are centered around λ_j^C for $j = 1, \ldots, N^C$, while the second set of discs are centered around $\tau \lambda_j^S + \mathrm{i}\gamma_j$ for $j = 1, \ldots, N^{NC}$. For sufficiently large τ, these disks must become disjoint, implying that the union of disks centered around λ_i^C contains exactly N^C eigenvalues, while the union of disks centered around λ_i^{NC} contain exactly N^{NC} eigenvalues [16]. In other words, the spectra of $\boldsymbol{K}$ diverges into two distinct sets of N^C and N^{NC} eigenvalues each as $\tau \to \infty$, with the set of N^{NC} eigenvalues containing negative real parts with magnitude $O(\tau)$.

Consider now the N^C eigenvalues with the smallest magnitude. By the Gerschgorin argument, these must remain bounded as $\tau \to \infty$. Let $\boldsymbol{W} = (\boldsymbol{W}^C, \boldsymbol{W}^{NC})$ and $\boldsymbol{\Lambda}^C$ be the matrix of eigenvectors and eigenvalues corresponding to these N^C smallest eigenvalues, such that

$$\begin{pmatrix} \boldsymbol{A} & \boldsymbol{B} \\ -\boldsymbol{B}^T & \boldsymbol{C} + \tau \boldsymbol{S} \end{pmatrix} \begin{pmatrix} \boldsymbol{W}^C \\ \boldsymbol{W}^{NC} \end{pmatrix} = \begin{pmatrix} \boldsymbol{A} \boldsymbol{W}^C + \boldsymbol{B} \boldsymbol{W}^{NC} \\ -\boldsymbol{B}^T \boldsymbol{W}^C + \boldsymbol{C} \boldsymbol{W}^{NC} + \tau \boldsymbol{S} \boldsymbol{W}^{NC} \end{pmatrix} = \boldsymbol{\Lambda}_C \begin{pmatrix} \boldsymbol{W}^C \\ \boldsymbol{W}^{NC} \end{pmatrix}$$

This implies

$$\tau \left\| \boldsymbol{S} \boldsymbol{W}^{NC} \right\| = \left\| \boldsymbol{\Lambda}^C \boldsymbol{W}^{NC} + \boldsymbol{B}^T \boldsymbol{W}^C - \boldsymbol{C} \boldsymbol{W}^{NC} \right\|.$$

Since $\boldsymbol{\Lambda}^C$ remains bounded as $\tau \to \infty$, the right hand side is bounded independently of τ under normalization of $\boldsymbol{W}^C, \boldsymbol{W}^{NC}$, implying that the non-conforming component $\boldsymbol{W}^{NC}$ satisfies

$$\sqrt{\lambda_{\min}^{NC}} \left\| \boldsymbol{W}^{NC} \right\| \leq \left\| \boldsymbol{S} \boldsymbol{W}^{NC} \right\| = O(1/\tau)$$

where $\lambda_{\min}^{NC} > 0$ is the smallest eigenvalue of $\boldsymbol{S}$. As a consequence, $\boldsymbol{W}^{NC} \to 0$ as $\tau \to \infty$, and the smallest N^C eigenvalues of $\boldsymbol{K}$ converge to the eigenvalues of $\boldsymbol{A}$ at a rate of $O(1/\tau)$. These correspond to a discretization using the conforming approximation space (4).

These results are summarized in the following lemma:

Lemma 3.1 *As $\tau \to \infty$, the spectrum of the DG discretization matrix $\boldsymbol{K}$ decouples into two sets of eigenvalues $\{\lambda_1^C, \ldots, \lambda_{N^C}^C\}$ and $\{\lambda_1^{NC}, \ldots, \lambda_{N^{NC}}^{NC}\}$. The eigenvalues $\{\lambda_1^{NC}, \ldots, \lambda_{N^{NC}}^{NC}\}$ diverge towards the left half plane, with $|\mathrm{Re}(\lambda_i)| = O(\tau)$, while the eigenvalues $\{\lambda_1^C, \ldots, \lambda_{N^C}^C\}$ converge to the eigenvalues of $\boldsymbol{A}$ at the rate $O(1/\tau)$.*

We note that, while we consider skew-symmetric DG formulations in this work, Lemma 3.1 is straightforward to generalize to any DG formulations where $\boldsymbol{S}$ is symmetric negative definite and $\boldsymbol{A}$ is diagonalizable.

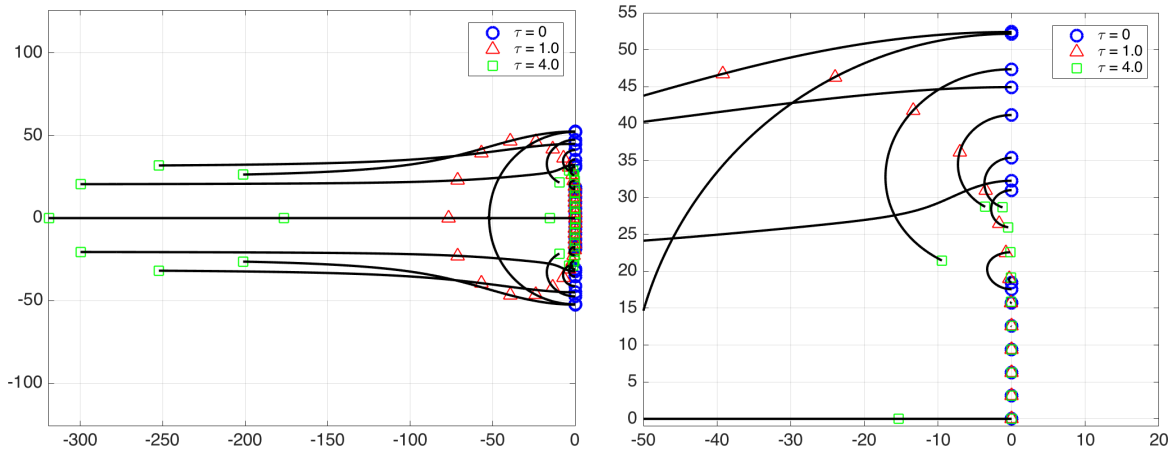

(a) Paths of eigenvalues as τ increases

(b) Zoom of eigenvalues near imaginary axis

Figure 1: Eigenvalue paths for DG advection with $\tau \in [0, 4]$ on a mesh of 8 elements of degree $N = 3$. Eigenvalues are overlaid on these paths for $\tau = 0$, $\tau = 1$, and $\tau = 4$. The zoomed in view near the imaginary axis shows the return of spurious modes to the imaginary axis for τ sufficiently large.

4 Numerical experiments

The above analysis illustrates the behavior of the spectra of the DG discretization for the asymptotic cases when $\tau = 0$ or $\tau \to \infty$. However, it is less clear how the spectra of $\boldsymbol{K}$ behaves for $\tau \approx 1$. We rely instead on numerical experiments in one and two space dimensions to illustrate behaviors for the advection and acoustic wave equations. In particular, these experiments indicate that certain modes with negative real part for $\tau = O(1)$ return to the imaginary axis as $\tau \to \infty$. Since eigenvalues with a negative real part correspond to dissipation in time-domain simulations, this implies that these under-resolved modes become undamped as τ grows sufficiently large.

4.1 1D experiments

We consider first the scalar advection equation in 1D with periodic boundary conditions. For $\tau = 0$, the eigenvalues of the DG discretization matrix are purely imaginary. Paths taken by eigenvalues as τ increases are determined by sampling spectra over a sufficiently fine set of τ and using a particle tracking method [17]. Figure 1 shows the paths taken by these eigenvalues as τ increases from zero to $\tau = 4$. As predicted, a subset of *divergent* eigenvalues move further left of the imaginary axis as τ increases. The corresponding eigenmodes are shown in Figure 2, with inter-element jumps of these eigenfunctions increasing as τ increases.

However, for sufficiently large τ, a subset of eigenvalues return to the imaginary axis. Figure 3 illustrates that, as τ increases, the magnitude of the inter-element jumps present in these modes decreases, and the mode approaches a C^0 continuous function. These eigenvalues which move right to return to the imaginary axis correspond to a second set of *spurious* modes. These modes are related to spurious modes observed for high order C^0 finite element methods [18], which consist of higher frequency components with sharp peaks. Since the real part of these eigenvalues approaches zero as $\tau \to \infty$, these modes become undamped and persist as spurious solution components in time-domain simulations [19]

We repeat the above experiment for the acoustic wave equation in 1D with reflection boundary conditions on $[-1, 1]$, and compare against the exact eigenvalues $\lambda_i = i\frac{\pi}{2}$ for $i = 1, 2, \ldots$. The behavior of the eigenvalues as τ increases (Figure 6) is similar to the behavior observed for the scalar advection equation. An examination of the eigenmodes corresponding to divergent and spurious eigenvalues as $\tau \to \infty$ shows that these modes behave similarly to the spurious modes observed for the scalar advection equation, with individual pressure

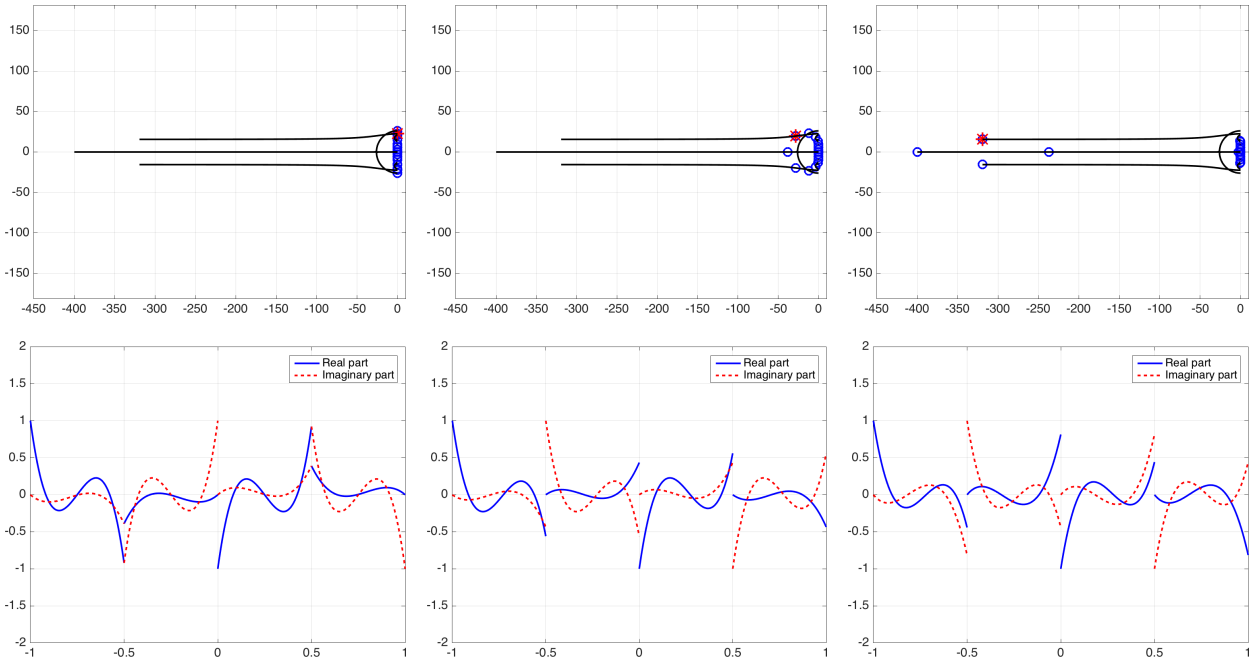

(d) $\tau = 0$ (e) $\tau = 1$ (f) $\tau = 10$

Figure 2: Behavior of divergent eigenvalues for advection as τ increases. The order of approximation is $N = 3$ on a mesh of 4 elements.

and velocity components converging to continuous functions.

4.2 2D experiments

In two space dimensions, taking $\tau \to \infty$ again results in spurious modes which return to the imaginary axis, with the corresponding eigenmodes approaching conforming functions. We illustrate this through numerical experiments for the acoustic wave equation and advection in two space dimensions. In all numerical experiments, we use $N = 3$ and a uniform triangular mesh resulting from bisecting each element of a 2×2 uniform quadrilateral mesh.

Figure 4 shows the spectra of the DG discretization matrix for the acoustic wave equation for $\tau = 1, 10, 50$. Like the one-dimensional case, a subset of eigenvalues diverge towards the left half plane as τ increases, though unlike the one-dimensional case, these eigenvalues collapse towards the real line as τ increases. Similarly, as predicted, a subset of eigenvalues returns towards the imaginary axis as $\tau \to \infty$. These are shown in Figure 5, along with traced paths taken by each eigenvalue as τ increases.

The pressure and velocity components of the corresponding acoustic eigenmodes converge to conforming approximations. As noted in Section 3.2, this implies that pressure components lie in $H^1(\Omega_h)$ and are continuous across faces, edges, and vertices. Figure 6 shows the behavior of the pressure component of an eigenmode corresponding to a spurious returning eigenvalue for $\tau = .1, 1, 100$. As τ increases and the eigenvalue approaches the imaginary axis, the eigenmode approaches a C^0 continuous function with a high frequencies and sharp peak, similar to the spurious eigenmodes observed for the one-dimensional case in Figure 3. Likewise, the non-zero velocity components of spurious eigenmodes converge to approximations in $H(\text{div}; \Omega_h)$, such that only the normal component of velocity is continuous across faces. Figure 7 shows visualizations of these eigenmodes. For large τ, normal jumps of the velocity component vanish.

For the advection equation with periodic boundary conditions, the spectra of the DG discretization behaves similarly. In all following experiments, we use advection vector $\beta = (1, 0)$. For $\tau = 0$, all eigenvalues

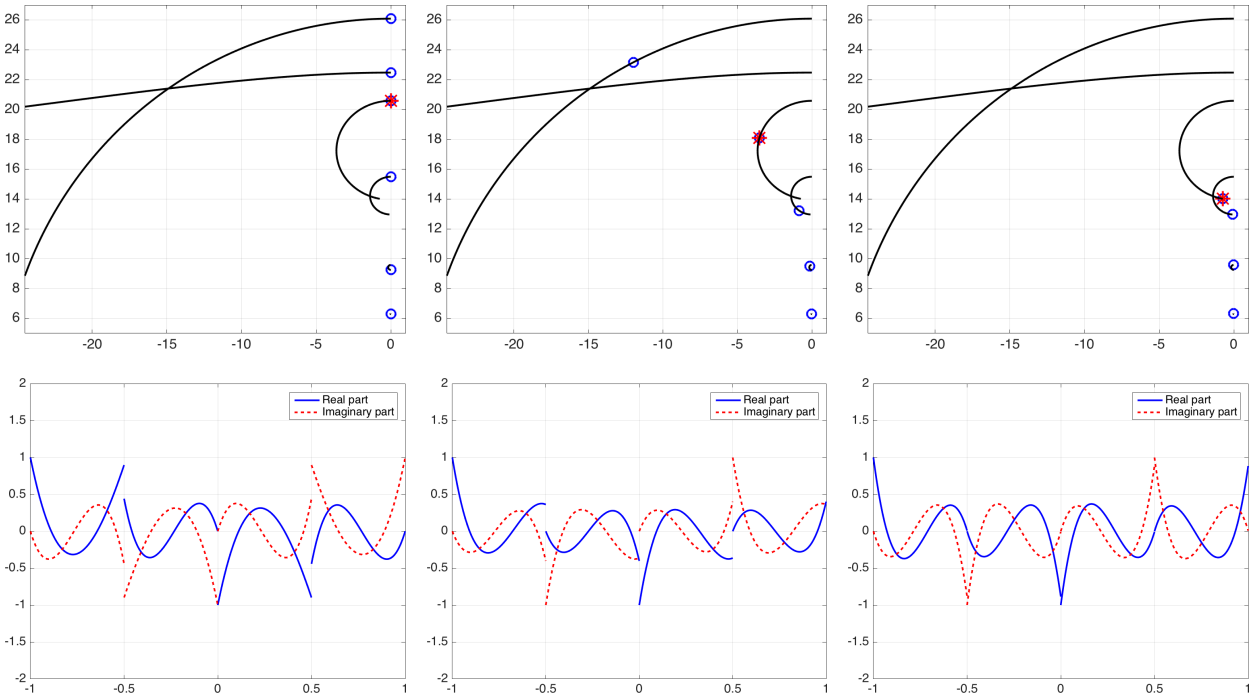

(d) $\tau = 0$ (e) $\tau = 1$ (f) $\tau = 10$

Figure 3: Return behavior of DG advection eigenvalues for sufficiently large τ. For $\tau = 1$ certain eigenvalues have negative real part, and the corresponding eigenmodes are damped. For $\tau \gg 1$, certain eigenvalues return to the imaginary axis as spurious modes in conforming discretizations.

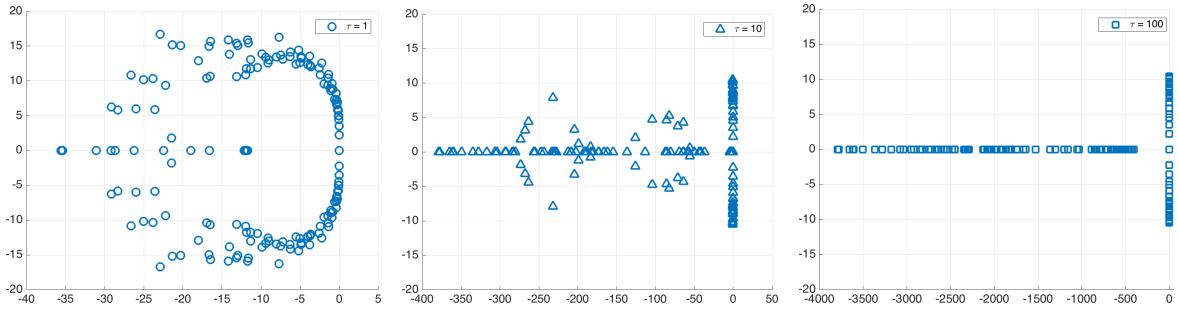

(a) $\tau = 1$ (b) $\tau = 10$ (c) $\tau = 100$

Figure 4: Behavior of eigenvalues for the acoustic wave equation in two dimensions. Note the changing scale of the real axis.

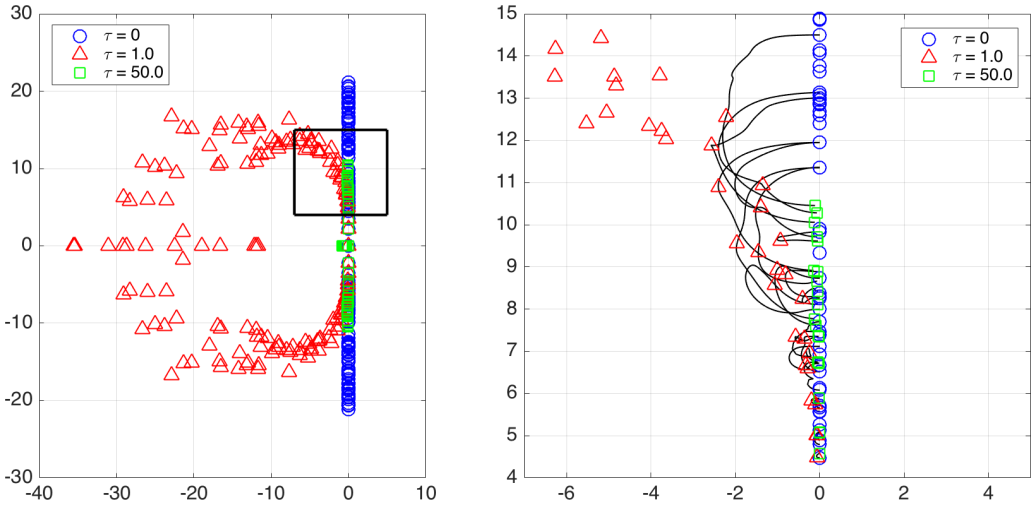

(a) $\tau = 0, 1, 50$, zoomed in view (b) $\tau = 0, 1, 50$, returning eigenvalue paths

Figure 5: Behavior of eigenvalues for the acoustic wave equation in two dimensions. Figure 5b shows a zoom of the boxed region in Figure 5a, with overlaid eigenvalue paths as τ increases. Divergent eigenvalues in the far left half plane are not shown.

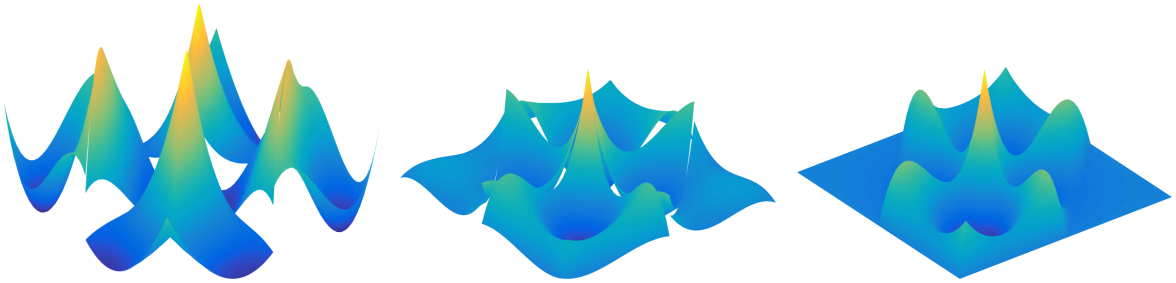

(a) $\tau = .1$, $\lambda = -0.2379 + 8.7528i$ (b) $\tau = 1$, $\lambda = -1.0145 + 8.9270i$ (c) $\tau = 100$, $\lambda = -0.0437 + 7.6167i$

Figure 6: Behavior of the real part of the pressure component of spurious eigenmodes for the acoustic wave equation in two dimensions.

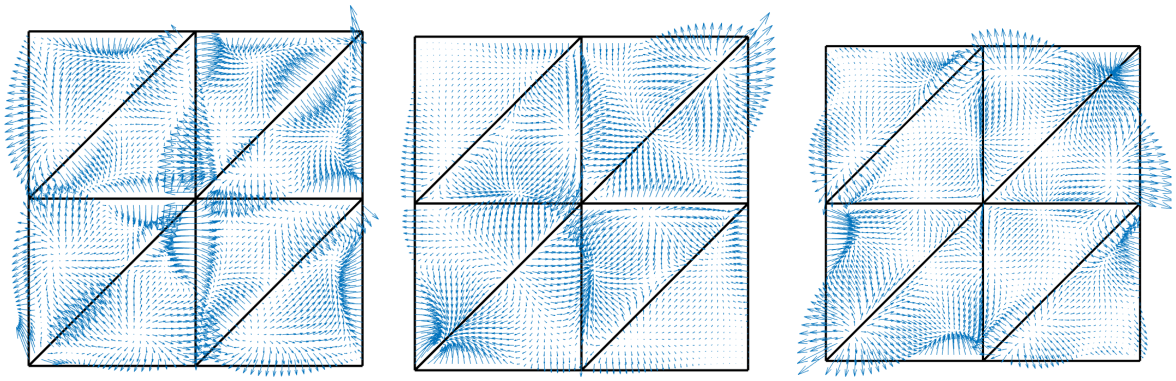

(a) $\tau = .1$, $\lambda = -0.6009 + 11.3209i$ (b) $\tau = 1$, $\lambda = -1.9601 + 9.5629i$ (c) $\tau = 100$, $\lambda = -0.0634 + 7.7670i$

Figure 7: Behavior of the real part of the velocity component of spurious eigenmodes for the acoustic wave equation in two dimensions.

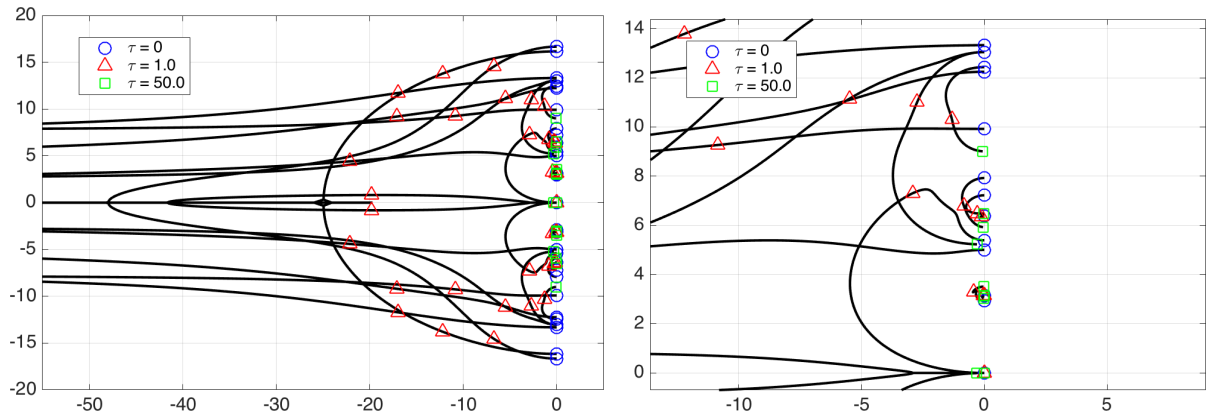

Figure 8: Eigenvalue paths for the DG discretization of advection as τ increases. Divergent eigenvalues in the far left half plane are not shown.

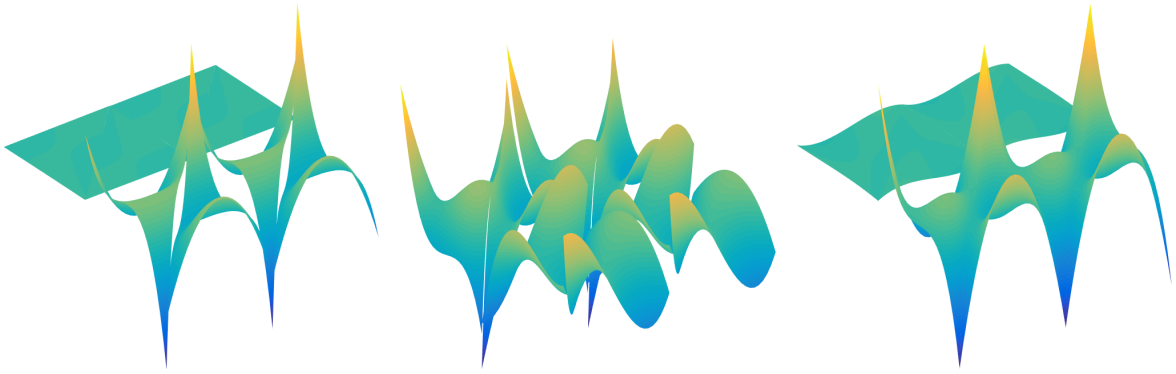

(a) $\tau = 0$, $\lambda = 0 + 7.9246i$ (b) $\tau = 1$, $\lambda = -0.8278 + 6.7831i$ (c) $\tau = 100$, $\lambda = -0.0239 + 5.9282i$

Figure 9: Behavior of the real part of spurious eigenmodes for the advection equation with $\beta = (1, 0)$.

lie on the imaginary axis, and as τ increases, the spectra splits into eigenvalues which diverge towards the left half plane and eigenvalues which return to the imaginary axis. Figure 8 shows the spectra of the DG matrix for $\tau = 0, 1, 50$, with eigenvalue paths for increasing values of τ overlaid.

Unlike spurious conforming modes present for the acoustic wave equation, spurious conforming modes for the advection equation satisfy $[\![\beta_n u]\!] = 0$, and allow discontinuities along faces which are tangential to flow directions, as shown in Figure 9.

5 Conclusions

For symmetric linear hyperbolic systems of PDEs, penalty fluxes are an alternative to upwind fluxes for DG methods. Both penalty and upwind fluxes can be interpreted as weakly enforcing continuity conditions implied by the underlying PDE. As the penalty parameter τ increases, we show that the eigenvalues of the DG discretization matrix split into two sets, with one set of eigenvalues converging to eigenvalues of a conforming discretization and the other set diverging with real part approaching $-\infty$.

Numerical experiments show that, for $\tau = O(1)$, there exist eigenvalues with negative real part which return to the imaginary axis as $\tau \to 0$ or $\tau \to \infty$. The corresponding eigenmodes of such eigenvalues can be interpreted as spurious under-resolved modes which persist in time-domain simulations. These results show

that the use of upwind and penalty fluxes damps such spurious modes present in both the limit of $\tau = 0$ (central fluxes) and $\tau \to \infty$ (a conforming discretization).

References

[1] Jesse Chan, Russell J Hewett, and T Warburton. Weight-adjusted discontinuous Galerkin methods: wave propagation in heterogeneous media. *arXiv preprint arXiv:1608.01944*, 2016.

[2] Jonás D De Basabe, Mrinal K Sen, and Mary F Wheeler. The interior penalty discontinuous Galerkin method for elastic wave propagation: grid dispersion. *Geophysical Journal International*, 175(1):83–93, 2008.

[3] Lucas C Wilcox, Georg Stadler, Carsten Burstedde, and Omar Ghattas. A high-order discontinuous Galerkin method for wave propagation through coupled elastic–acoustic media. *Journal of Computational Physics*, 229(24):9373–9396, 2010.

[4] Ruichao Ye, Maarten V de Hoop, Christopher L Petrovitch, Laura J Pyrak-Nolte, and Lucas C Wilcox. A discontinuous Galerkin method with a modified penalty flux for the propagation and scattering of acousto-elastic waves. *Geophysical Journal International*, 205(2):1267–1289, 2016.

[5] Jan S Hesthaven and T. Warburton. Nodal high-order methods on unstructured grids: I. time-domain solution of Maxwell's equations. *Journal of Computational Physics*, 181(1):186–221, 2002.

[6] Marcus J Grote, Anna Schneebeli, and Dominik Schötzau. Interior penalty discontinuous Galerkin method for Maxwell's equations: Energy norm error estimates. *Journal of Computational and Applied Mathematics*, 204(2):375–386, 2007.

[7] T. Warburton. A low-storage curvilinear discontinuous Galerkin method for wave problems. *SIAM Journal on Scientific Computing*, 35(4):A1987–A2012, 2013.

[8] E Diego Mercerat and Nathalie Glinsky. A nodal high-order discontinuous Galerkin method for elastic wave propagation in arbitrary heterogeneous media. *Geophysical Journal International*, 201(2):1101–1118, 2015.

[9] Jan S Hesthaven and Tim Warburton. *Nodal discontinuous Galerkin methods: algorithms, analysis, and applications*, volume 54. Springer, 2007.

[10] Franco Brezzi, Jim Douglas Jr, and L Donatella Marini. Two families of mixed finite elements for second order elliptic problems. *Numerische Mathematik*, 47(2):217–235, 1985.

[11] Daniele Boffi, Franco Brezzi, Michel Fortin, et al. *Mixed finite element methods and applications*, volume 44. Springer, 2013.

[12] Robert C Kirby. Algorithm 839: FIAT, a new paradigm for computing finite element basis functions. *ACM Transactions on Mathematical Software (TOMS)*, 30(4):502–516, 2004.

[13] T. Warburton and Mark Embree. The role of the penalty in the local discontinuous Galerkin method for Maxwell's eigenvalue problem. *Computer Methods in Applied Mechanics and Engineering*, 195(25-28):3205 – 3223, 2006.

[14] Jesse Chan, Zheng Wang, Axel Modave, Jean-Francois Remacle, and T Warburton. GPU-accelerated discontinuous Galerkin methods on hybrid meshes. *Journal of Computational Physics*, 318:142–168, 2016.

[15] David A Kopriva and Gregor J Gassner. An energy stable discontinuous Galerkin spectral element discretization for variable coefficient advection problems. *SIAM Journal on Scientific Computing*, 36(4):A2076–A2099, 2014.

[16] Roger A Horn and Charles R Johnson. *Matrix analysis*. Cambridge university press, 2012.

[17] A simple multiple particle tracker with gap closing. `https://www.mathworks.com/matlabcentral/fileexchange/34040-simple-tracker`. Accessed 10/1/2016.

[18] Mark Ainsworth. Dispersive behaviour of high order finite element schemes for the one-way wave equation. *Journal of Computational Physics*, 259:1–10, 2014.

[19] Thomas JR Hughes, John A Evans, and Alessandro Reali. Finite element and NURBS approximations of eigenvalue, boundary-value, and initial-value problems. *Computer Methods in Applied Mechanics and Engineering*, 272:290–320, 2014.